

Determination of s - and p -wave $I = 1/2$ $K\pi$ scattering amplitudes in $N_f = 2 + 1$ lattice QCD

Ruairí Brett^a, John Bulava^b, Jacob Fallica^c, Andrew Hanlon^d, Ben Hörz^e,
Colin Morningstar^a

^a Department of Physics, Carnegie Mellon University, Pittsburgh, PA 15213, USA

^b Dept. of Mathematics and Computer Science and CP3-Origins, University of Southern Denmark,
Campusvej 55, 5230 Odense M, Denmark

^c Department of Physics and Astronomy, University of Kentucky, Lexington, KY 40506, USA

^d Helmholtz-Institut Mainz, Johannes Gutenberg-Universität, 55099 Mainz, Germany

^e PRISMA Cluster of Excellence and Institute for Nuclear Physics, Johannes Gutenberg-Universität,
55099 Mainz, Germany

Abstract

The elastic $I = 1/2$, s - and p -wave kaon-pion scattering amplitudes are calculated using a single ensemble of anisotropic lattice QCD gauge field configurations with $N_f = 2 + 1$ flavors of dynamical Wilson-clover fermions at $m_\pi = 230$ MeV. A large spatial extent of $L = 3.7$ fm enables a good energy resolution while partial wave mixing due to the reduced symmetries of the finite volume is treated explicitly. The p -wave amplitude is well described by a Breit-Wigner shape with parameters $m_{K^*}/m_\pi = 3.808(18)$ and $g_{K^*K\pi}^{\text{BW}} = 5.33(20)$ which are insensitive to the inclusion of d -wave mixing and variation of the s -wave parametrization. An effective range description of the near-threshold s -wave amplitude yields $m_\pi a_0 = -0.353(25)$.

Keywords: lattice QCD, meson scattering

PACS: 12.38.Gc, 11.15.Ha, 11.30.Rd, 13.30.Eg, 13.75.Lb, 13.85.Dz, 14.40.Be

1 Introduction

Elastic $K\pi$ scattering amplitudes are essential to several current frontiers in the phenomenology of the Standard Model of particle physics. For example, precision tests of lepton universality performed at CERN by the LHCb collaboration using decays in which the elastic $I(J^P) = \frac{1}{2}(1^-)$ $K^*(892)$ resonance is produced exhibit deviations between theory and experiment in $R_{K^*} = \text{BR}(B \rightarrow K^* \mu^+ \mu^-)/\text{BR}(B \rightarrow K^* e^+ e^-)$ at the $(2.1 - 2.5)\sigma$ level [1]. Although the hadronic form factors involved in these branching fractions cancel in the ratio, precise lattice QCD predictions are desirable. Existing lattice calculations of these form factors however do not treat the K^* as an unstable particle [2,3]. The theoretical formalism to extract form factors correctly treating the unstable nature of the K^* is well known [4,5] and requires the elastic p -wave $K\pi$ scattering amplitude calculated in this work.

In addition to the $K^*(892)$ resonance, the nature and existence of the low-lying broad s -wave $K_0^*(800)$ resonance is not clear [6]. The amplitudes calculated in this work may provide information on the quark-mass dependence of these resonance poles and confront expectations from chiral effective theories [7,8].

Finally, apart from study of the resonances, the $K\pi$ s -wave scattering lengths are of phenomenological interest as a precision Standard Model test. The DIRAC experiment at CERN has produced promising results for these quantities using πK ‘atoms’ and plans to achieve 5% accuracy [9]. The $I = 1/2$, s -wave scattering length calculated in this work is therefore an important step toward an accurate and precise determination of these scattering lengths using lattice QCD.

While lattice QCD is a proven tool to determine hadronic properties from first principles, real-time hadron-hadron scattering amplitudes are significantly more difficult to calculate than single-hadron properties due to the Euclidean space-time lattice [10]. However, a particularly successful approach developed by Lüscher circumvents this difficulty by inferring elastic scattering amplitudes from the deviation of finite-volume hadron-hadron energies from their non-interacting values [11]. This method has been extended to moving frames [12], particles with spin [13–16], and coupled two-hadron channels [17]. Progress toward the full extension to three-hadron amplitudes has been made in Refs. [18–26] and amplitudes with an external current can also be calculated [5,27–31]. Alternative approaches to handle inclusive decays which do not employ the finite volume have been proposed recently in Refs. [32,33].

In addition to this theoretical progress, algorithmic advances [34,35] and Moore’s law have resulted in considerable progress in lattice QCD calculations of finite-volume hadron-hadron energy spectra, and thus by extension scattering amplitudes as well. The state of such calculations has been reviewed recently in Ref. [36]. Lattice determinations of elastic meson-meson amplitudes are increasingly precise [37–60] while those of meson-baryon and baryon-baryon systems have considerably larger errors [61–66]. First results with coupled meson-meson channels have also been performed [67–72].

The $K\pi$ amplitudes described in this work present additional difficulties compared to the $\pi\pi$ case. Due to the reduced symmetry (compared to infinite volume) of the finite toroidal volume in which our simulations are performed, partial wave amplitudes with different orbital angular momenta contribute to the energy shift of a single finite-volume energy. The pattern of this partial wave mixing is more complicated at non-zero total mo-

$(L/a_s)^3 \times (T/a_t)$	N_{cfgs}	$a_t m_\pi$	$a_t m_K$	$a_t m_\eta$	ξ
$32^3 \times 256$	412	0.03938(19)	0.08354(15)	0.1010(37)	3.451(11)

Table 1: Details of the ensemble used in this work. Pion and kaon masses are taken from Ref. [60] while the determination of m_η is discussed in the text. The renormalized anisotropy ξ is set using the pion dispersion relation and also taken from Ref. [60]. Setting the scale with the kaon mass gives $a_t = 0.033357(59)\text{fm}$.

mentum if the hadrons are not identical. A practical theoretical and statistical treatment of these effects has been proposed recently in Ref. [14], which details the procedure we follow here.

The main results of this work are parametrizations of the s - and p -wave $I = 1/2$ elastic $K\pi$ scattering amplitudes. The p -wave amplitude is well-described by a Breit-Wigner, as expected in the presence of a narrow $K^*(892)$ resonance while the energy dependence of the s -wave amplitude can be fit with several ansatze including a Breit-Wigner. All parameters from these fits are listed in Tab. 5 and plots of several of them are shown in Fig. 5. In addition to these parametrizations, we provide in Tab. 4 the finite-volume energies and box matrix elements (which are defined in Eq. 2.6) to enable additional future parametrizations.

The remainder of this paper is organized as follows. In Sec. 2 we outline the ensemble of gauge field configurations, methods for calculating finite-volume two-hadron energies, and the relation of those energies to infinite volume scattering amplitudes. This is followed by Sec. 3, where results are presented, and Sec. 4 which contains conclusions.

2 Methods

We employ the single ensemble of anisotropic $N_f = 2 + 1$ Wilson clover fermions used previously in Ref. [60] for elastic pion-pion scattering. Much of the procedure developed there to determine the finite-volume two-hadron energies is taken over in this work. However, the relation of finite-volume energies to the desired amplitudes is complicated significantly with respect to Ref. [60] so the analysis methods proposed in Ref. [14] must be employed.

2.1 Ensemble Details

The ensemble of anisotropic gauge configurations used in this work is detailed in Refs. [73, 74] but we review the salient points here. The gauge action is Symanzik and tadpole improved at tree level and a clover term is added to the Wilson action for fermions. The spatial gauge links appearing in the fermion action are stout smeared. Properties of the ensemble relevant for this work are listed in Tab. 1. While all our dimensionful results are expressed as dimensionless ratios using m_π , an indicative value of the lattice scale is obtained (as in Ref. [60]) by demanding that the kaon mass take its physical value. Such a (mass-dependent) scale setting gives $a_t = 0.033357(59)\text{fm}$.

This work is based on $N_{\text{cfg}} = 412$ configurations which are separated by 20 Hybrid Monte Carlo (HMC) trajectories of length $\tau = 1$. While no statistically significant auto-correlations are observed in any of the correlation functions we consider here, in order to

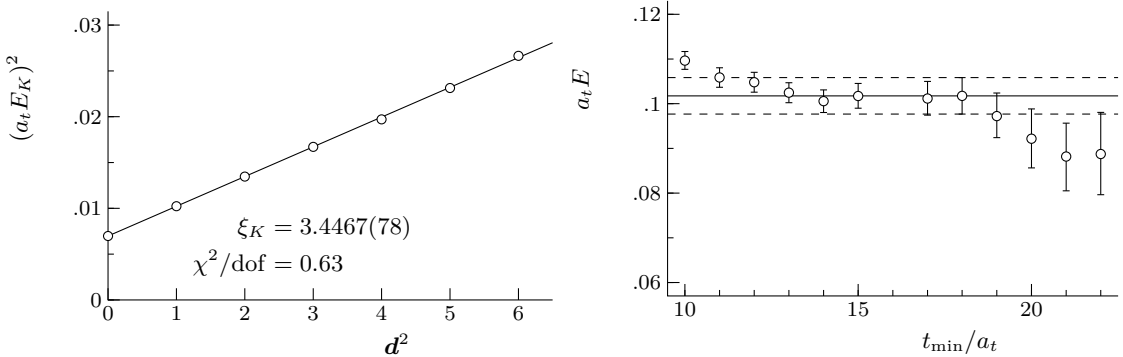


Figure 1: **Left:** linear fit to the energies of single-kaon correlation functions to determine the kaon anisotropy ξ_K , which is consistent with ξ_π from the pion dispersion relation. **Right:** t_{\min} -plot for the determination of m_η with $t_{\max} = 26a_t$. This analysis involves a GEVP and is discussed further in the text.

mitigate the effect of autocorrelation on our estimates of the statistical error we bin the data in bins of size $N_{\text{bin}} = 2$. Using this binned data set, statistical errors are estimated using the bootstrap procedure with $N_B = 800$ bootstrap samples.

Determination of the pion and kaon masses is discussed in Ref. [60] and we take over those values here. We additionally employ the renormalized anisotropy ($\xi = a_s/a_t = \xi_\pi$) determined in Ref. [60] by enforcing the correct relativistic dispersion relation for the pion. As discussed in Ref. [71], ξ is insensitive to the hadron whose dispersion relation is used. For example, our determination of ξ_K using the kaon dispersion relation is shown in Fig. 1 and agrees well with ξ_π . The linear fit used to determine ξ_K is shown in Fig. 1, in which the individual energies are obtained from single-exponential fits to the relevant correlation functions which ignore the finite temporal extent T . As demonstrated in Ref. [60], at the current level of statistical precision, we find that finite- T effects are negligible. These single exponential fits are performed over a range $[t_{\min}, t_{\max}]$, so that the level of unwanted excited state contamination can be monitored by varying t_{\min} . If the fitted energies do not exhibit statistically significant variation for a range of t_{\min} , systematic errors due to excited states are smaller than the statistical errors. The t_{\min} plots illustrating these plateaux for all single- K levels used in determining ξ_K are shown in Fig. 7 of App. A. We also check that finite- T effects are small by observing that energies obtained from fit form $A \exp(-Et)$ are indistinguishable from those obtained using fit form $A[\exp(-Et) + \exp(-E(T-t))]$ plus other terms that can occur in two-meson correlators.

In addition to the pion and kaon masses, we require an estimate of m_η . These three hadron masses determine the position of relevant inelastic thresholds for $I = 1/2$, $S = 1$ kaon-pion scattering, which is the focus of this work. To determine m_η , we solve a generalized eigenvalue problem (GEVP) which includes two single-site interpolating operators with flavor content $\bar{u}u + \bar{d}d$ and $\bar{s}s$. The GEVP

$$C(t_d) v(t_0, t_d) = \lambda(t_0, t_d) C(t_0) v(t_0, t_d) \quad (2.1)$$

is solved once for a single choice of the diagonalization times $(t_0, t_d) = (9a_t, 18a_t)$, where $C(t)$ is the 2×2 correlation matrix composed of the light and strange interpolators. The eigenvector corresponding to the largest eigenvalue is used to rotate the correlation matrix

	$a_t E_{\text{th}}$	E_{th}/m_π	$(E_{\text{th}} - m_K)/m_\pi$
πK	0.12293(24)	3.121(11)	1
$\pi\pi K$	0.16233(40)	4.121(11)	2
ηK	0.1845(37)	4.664(99)	2.553(96)

Table 2: Relevant inelastic thresholds for $I = \frac{1}{2}$, $S = 1$ kaon-pion scattering. Since the lowest inelastic threshold contains three hadrons, we treat elastic scattering only.

and obtain a single diagonal correlation function which has optimal overlap onto the ground state [75]. Single exponential fits to this optimized ground state correlation function for varying t_{min} are displayed in Fig. 1. These fitted energies vary little with (t_0, t_d) and are insensitive to an enlargement of the GEVP operator basis. As a flavor singlet, η -meson correlation functions contain fully disconnected quark lines, our estimation of which is discussed in Sec. 2.2. These relative quark lines start and end at the same time and are estimated using non-maximal time dilution, in which each dilution projector has support on every sixteenth timeslice. Since we only employ a single combination of stochastic sources, our estimate of η -meson correlation functions at a separation of precisely $t = 16a_t$ is poorly estimated compared to the other points. Time separation $t = 16a_t$ is therefore removed from all fits to η -meson correlators.

Using the masses m_π , m_K , and m_η the relevant inelastic thresholds are given in Tab. 2. While the formalism discussed in Sec. 2.4 can relate energies above inelastic two-hadron thresholds to the corresponding coupled-channel scattering amplitude, the situation above three-hadron thresholds is more complicated [21, 25]. On this ensemble $\pi\pi K$ is the lowest inelastic threshold and sits below ηK , so we are able to treat elastic πK scattering only. A convenient parameter delineating the elastic region is $\tilde{E} = (E_{\text{cm}} - m_K)/m_\pi$. As indicated in the table, the elastic region of interest extends over the range $1 < \tilde{E} < 2$.

2.2 Correlation function construction

As discussed in Sec. 2.4, infinite volume elastic scattering amplitudes are related to finite-volume two-hadron energies. These energies are determined in lattice QCD simulations by fitting the exponential fall-off of temporal correlation functions between suitable interpolating operators. In order to employ two-hadron interpolating operators in which each hadron has definite momentum, and to treat Wick contractions where some quark lines start and end at the same time, all-to-all quark propagators between each spacetime point are required.

Such all-to-all propagators are intractable to evaluate directly but efficient stochastic estimators can be constructed for propagators projected onto the space spanned by the N_{ev} lowest eigenmodes of the (stout-smeared) gauge-invariant three-dimensional Laplace operator [34, 35]. We refer to this as the LapH subspace and this projection is simply a particular form of quark smearing, which has long been used to reduce the amount of unwanted excited state overlap in hadronic interpolating operators.

These stochastic estimators introduce noise into the LapH subspace and may be improved via dilution [76], in which a set of complete orthogonal projectors is specified in time, spin, and Laplacian eigenvector indices. We differentiate quark lines which start

\mathbf{d}	Λ	ℓ
$(0, 0, 0)$	A_{1g}	$0, 4, \dots$
	T_{1u}	$1, 3, \dots$
$(0, 0, n)$	A_1	$0, 1, 2, \dots$
	E	$1, 2, 3, \dots$
$(0, n, n)$	A_1	$0, 1, 2, \dots$
	B_1	$1, 2, 3, \dots$
	B_2	$1, 2, 3, \dots$
(n, n, n)	A_1	$0, 1, 2, \dots$
	E	$1, 2, 3, \dots$

Table 3: Irreps Λ of the appropriate little group for various total momenta $\mathbf{P}_{\text{tot}} = (2\pi/L)\mathbf{d}$ (where \mathbf{d} is a vector of integers) considered in this work. We consider $K\pi$ systems at rest as well as those with non-zero total on-axis, planar-diagonal, and cubic-diagonal momenta. These momentum classes are listed in the first column, where $n \in \mathbb{Z}$ is an arbitrary integer.

and end at the same time (relative lines) from those which start and end at different times (fixed lines), and it is beneficial to adopt different dilution schemes for fixed and relative lines. For this work we employ the same quark smearing ($N_{\text{ev}} = 264$) and dilution schemes as Ref. [60]. In addition to the light quark inversions performed there, we require a single independent fixed strange line. All correlators are estimated using a minimal number of stochastic sources, and only a single permutation of these sources is employed. Although additional Dirac matrix inversions are performed in order to construct correlators for other systems, the results of this work employ three fixed light quark lines, one fixed strange quark line, and a single relative light quark line. Given the dilution schemes employed here, this work therefore requires $N_{\text{light}} = 1280$ light Dirac matrix inversions and $N_{\text{strange}} = 256$ strange inversions on each gauge configuration. The determination of m_η discussed in Sec. 2.1 additionally uses a single relative strange line requiring another $N_{\text{strange}} = 512$ strange inversions.

Using the source and sink functions defined in Ref. [35], all Wick contractions (also enumerated in Ref. [35]) for correlation functions between single-meson and meson-meson interpolators may be efficiently evaluated. The single-meson and meson-meson operators employed here are taken from Ref. [77] and transform irreducibly according to the appropriate finite-volume symmetry group. We consider πK operators at zero total momentum $\mathbf{d}^2 = (L/2\pi)^2 \mathbf{P}_{\text{tot}}^2$ as well as all non-zero on-axis, planar-diagonal, and cubic diagonal total momenta up to $\mathbf{d}^2 \leq 4$.

Our interpolating operators therefore transform irreducibly according to the appropriate little group for each total momentum ray. Due to the reduced symmetry of the finite periodic spatial volume, a single infinite-volume irrep (labeled by orbital angular momentum ℓ) will be subduced onto possibly several finite volume irreps, which are denoted by Λ . The ℓ th partial wave may also occur multiple times in a particular finite volume irrep. This subduction pattern is illustrated in Tab. 3 for the irreps considered in this work. Increased complication with respect to the pion-pion case due to non-identical

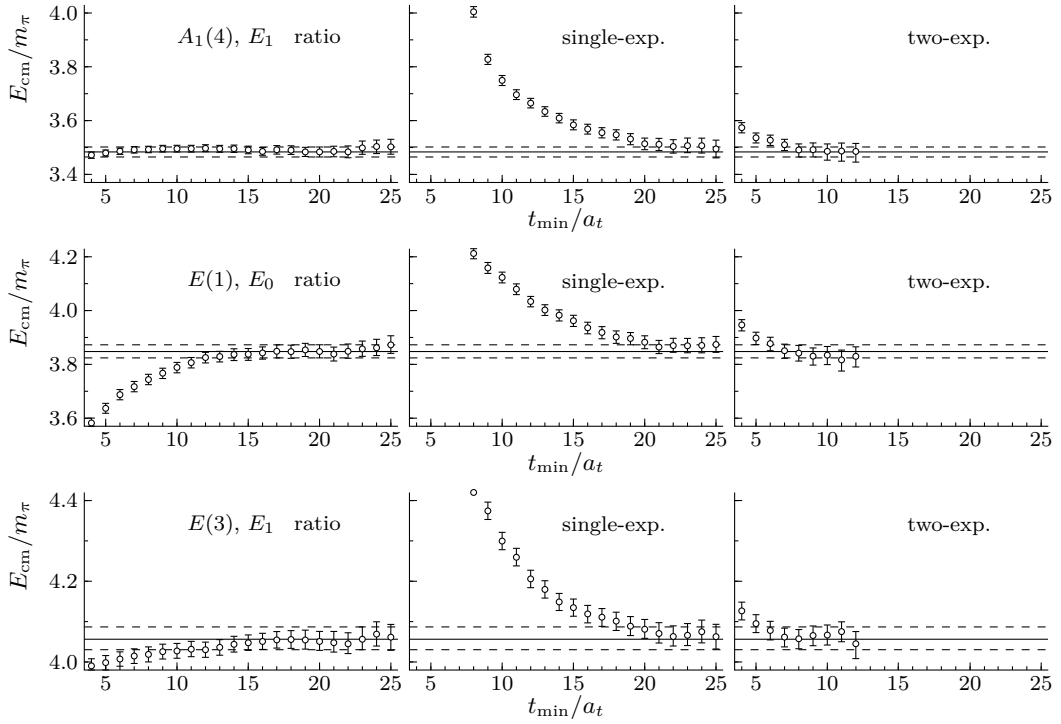


Figure 2: Comparison of ratio, single exponential, and two-exponential fits for a selection of levels throughout the elastic region. Each row corresponds to the three fits for a single level specified in the left column as ‘ $\Lambda(d^2), E_n$ ’, denoting the n th level in finite volume irrep Λ with total momentum d^2 . Each plot shows the variation of the fitted energy with t_{\min} , the lower end of the fitting range.

particles is now evident. While even and odd partial waves do not contribute to the same irrep at zero total momentum, there are no non-zero momentum irreps to which $\ell = 0$ contributes but not $\ell = 1$.

In each of the irreps listed in Tab. 3, we form a temporal correlation matrix from which the finite-volume spectrum is extracted. Assuming the presence of a narrow $K^*(892)$ resonance and allowing for the possibility of an additional s -wave resonance, these correlation matrices are composed of (non-displaced) single-hadron operators as well as kaon-pion operators with various individual momenta. Using estimates based on m_K , m_π and L , roughly 2 – 6 irreducible $K\pi$ interpolating operators corresponding to the lowest non-interacting states are included in each irrep, together with 1 – 2 single-hadron operators. These operators are intended to have large overlap onto all elastic states of interest, as well as a few states above inelastic threshold. Using a larger basis than strictly necessary enables a check of the stability of the spectrum as a few higher-lying operators are removed. Full specification of the operators included in each irrep is given in App. B.

2.3 Finite-Volume Spectrum Determination

Given the correlation matrices discussed in Sec. 2.2, we turn now to methods for extracting finite-volume spectra from them. As discussed in Sec. 2.1 in the determination of single hadron masses, we can safely neglect finite temporal extent effects. Since several

excited states are desired in addition to the ground state in each irrep, GEVP methods are employed which solve Eq. 2.1 once for a single choice of (t_0, t_d) and a correlation matrix of size N_{op} . The operators included in the GEVP are given in Tab. 6 in App. B. Any variation of the spectrum with (t_0, t_d) and N_{op} implies a systematic uncertainty whose magnitude must be assessed.

Using the GEVP eigenvectors $\{v_n\}$ the correlation matrix is rotated

$$\hat{C}_n(t) = (v_n, C(t)v_n), \quad (2.2)$$

where the outer parentheses on the RHS denote an inner product over the GEVP index. $\hat{C}_n(t)$ is a diagonal correlation function with optimal overlap onto finite-volume energy level n [75]. As discussed in Sec. 2.4, the signal of interest is the deviation of the finite-volume two-hadron energies from their non-interacting counterparts. To this end, the energy difference ΔE is extracted directly by constructing the ratio

$$R_n(t) = \frac{\hat{C}_n(t)}{C_\pi(\mathbf{d}_\pi^2, t) C_K(\mathbf{d}_K^2, t)} \quad (2.3)$$

where the nearest non-interacting state to energy level n consists of a pion with momentum \mathbf{d}_π^2 and a kaon with momentum \mathbf{d}_K^2 . Single-exponential correlated- χ^2 fits are performed to the ansatz $R_n(t) = A_n e^{-\Delta E_n t}$.

For weakly interacting levels where ΔE_n is small, these ratio fits generally have considerably smaller excited contamination than fits to $\hat{C}_n(t)$ directly. However, the identification of plateau with the ratio fits is complicated somewhat because the contributions from unwanted higher-lying states do not necessarily enter with a positive sign, as they do in $\hat{C}_n(t)$ [60]. These ‘bumps’ are evident in t_{min} -plots for levels which exhibit significant deviation from the non-interacting energies. Nonetheless, taking these bumps into account results in consistent energies and statistical errors for these levels between ratio fits and exponential fits to $\hat{C}_n(t)$. Ratio fits are compared to fits to $\hat{C}_n(t)$ directly using single-exponential and two-exponential ansatze in Fig. 2.

As in Ref. [60] ratio fits are employed for the final amplitude analysis. Similar to the single-hadron operator fits discussed in Sec. 2.1, t_{min} must be chosen so that systematic errors due to unwanted excited state contamination are smaller than statistical ones. For these fits we additionally require that any variation with (t_0, t_d) or N_{op} is also smaller than the statistical error. Generally the variation of the energies with the GEVP parameters is small, as illustrated in Fig. 3.

2.4 Amplitudes from finite-volume energies

After determining ΔE_n as described in Sec. 2.3, we reconstruct the finite volume energies via

$$a_t E_n = a_t \Delta E_n + \sqrt{a_t^2 m_\pi^2 + \left(\frac{2\pi a_s}{\xi L}\right)^2 \mathbf{d}_\pi^2} + \sqrt{a_t^2 m_K^2 + \left(\frac{2\pi a_s}{\xi L}\right)^2 \mathbf{d}_K^2}. \quad (2.4)$$

These energies are determined in the ‘lab’ frame in which the $K\pi$ system may have non-zero total momentum. These lab-frame energies are related to quantities in the center-of-mass frame by

$$E_{\text{cm}} = \sqrt{E^2 - \mathbf{P}_{\text{tot}}^2}, \quad q_{\text{cm}}^2 = \frac{1}{4} E_{\text{cm}}^2 - \frac{1}{2} (m_\pi^2 + m_K^2) + \frac{(m_\pi^2 - m_K^2)^2}{4 E_{\text{cm}}^2}, \quad (2.5)$$

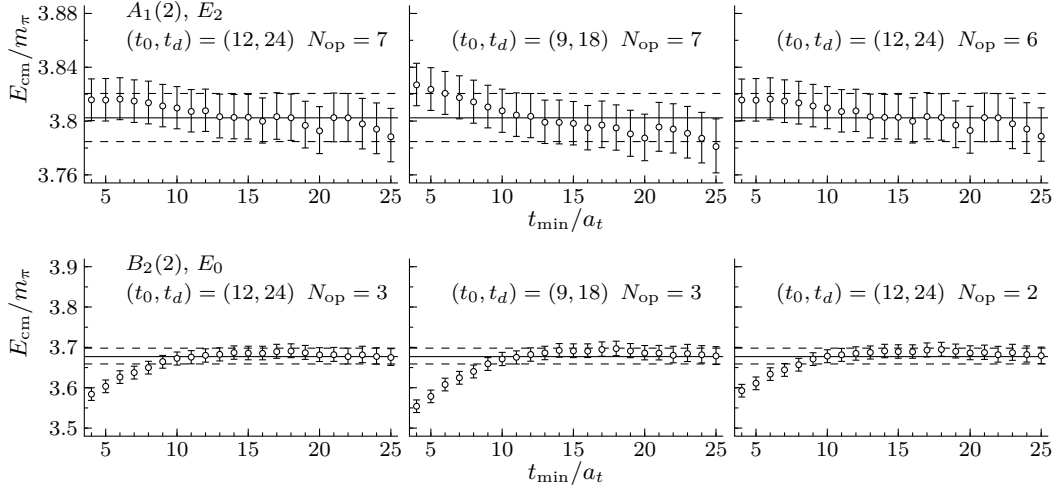


Figure 3: Comparison of ratio fits for different GEVP parameters for a selection of levels. As in Fig. 2, each row corresponds to a different energy, denoted in the left column. The GEVP bases are given in Tab. 6 where bases with one fewer operator are formed by discarding the last entry in each operator list. Each plot shows the variation of the fitted energy with t_{\min}/a_t , the lower end of the fitting range. GEVP systematics for all other levels are less pronounced than those shown here.

where E is the lab frame energy.

The relation between two-particle center-of-mass energies and the infinite-volume elastic scattering amplitude may be expressed as [14]

$$\det[\tilde{K}^{-1}(E_{\text{cm}}) - B^{(\Lambda, \mathbf{d})}(E_{\text{cm}})] = 0 \quad (2.6)$$

which holds up to corrections which are exponentially suppressed in the spatial extent L . For the elastic scattering of two spinless particles, \tilde{K}^{-1} and B are infinite-dimensional matrices in both ℓ and n_{occ} , an index enumerating the possibly multiple occurrences of a single partial wave in a particular irrep. Note that B depends on the total momentum class and irrep. Expressions and numerical programs for evaluation of the B -matrix elements are provided in Ref. [14].

For a unitary elastic scattering matrix S , the K -matrix is real, symmetric, and diagonal in ℓ and n_{occ} . It is related to the S -matrix by

$$K = (2T^{-1} + i)^{-1}, \quad S = 1 + iT,$$

while for spinless particles \tilde{K}^{-1} is defined as

$$\tilde{K}_{\ell}^{-1}(E_{\text{cm}}) = \left(\frac{q_{\text{cm}}}{m_{\pi}}\right)^{2\ell+1} K_{\ell}^{-1}(E_{\text{cm}}) = \left(\frac{q_{\text{cm}}}{m_{\pi}}\right)^{2\ell+1} \cot \delta_{\ell}(E_{\text{cm}}) \quad (2.7)$$

and is expected to be smooth near the elastic threshold. In this work the elements of \tilde{K} are made dimensionless using m_{π} , which is a different convention for \tilde{K} and B compared to Eqs. 18 and 20 of Ref. [14] which uses $2\pi/L$.

When employing the determinant condition in Eq. 2.6 to the irreps listed in Tab. 3, partial wave mixing must be treated carefully. In order to proceed, we first neglect all

partial waves with $\ell \geq 2$. The systematic error due to this truncation will be assessed shortly. After applying this restriction the B -matrices appearing in Eq. 2.6 are either one- or two-dimensional. For a one-dimensional B -matrix the determinant condition is of course trivial and yields a one-to-one relationship between a finite-volume energy E_{cm} and an amplitude point $\tilde{K}_\ell^{-1}(E_{\text{cm}})$. This one-to-one relationship is typically exploited in calculations of elastic pion-pion scattering amplitudes.

While there are a number of irreps listed in Tab. 3 for which the $\ell = 1$ partial wave can be isolated in this manner, is it only the A_{1g} irrep at zero total momentum (denoted $A_{1g}(0)$) which provides unambiguous s -wave amplitude points. Therefore, we proceed with the determination of both amplitudes by simultaneously fitting the elastic energies in all irreps according to the method of Ref. [14]. For these global fits, a parametrization of the s - and p -waves are required which describes $\tilde{K}_\ell^{-1}(E_{\text{cm}})$ using a few fit parameters. These parameters are determined by minimizing a correlated χ^2 which consists of residuals given by the determinants in Eq. 2.6. Ref. [14] also proposes another option for the residuals, namely

$$\Omega(\mu, A) = \frac{\det(A)}{\det[(\mu^2 + AA^\dagger)^{1/2}]}, \quad (2.8)$$

where $A = \tilde{K}^{-1} - B$ is the matrix appearing in the determinant, and μ is an arbitrary parameter chosen to suppress unimportant contributions to the determinant, which also improves the convergence of the minimization procedure. The residuals in Eq. 2.8 are constructed to efficiently treat large-dimensional matrices, but we employ them here as consistency checks with the determinant-residual fits.

Suitable parametrizations for these amplitudes are now discussed. Based on the expectation of a narrow $K^*(892)$ resonance, the p -wave amplitude is parametrized by a relativistic Breit-Wigner

$$(\tilde{K}_1^{-1})^{\text{BW}}(E_{\text{cm}}) = \left(\frac{m_{K^*}^2}{m_\pi^2} - \frac{E_{\text{cm}}^2}{m_\pi^2} \right) \frac{6\pi E_{\text{cm}}}{g_{K^*\pi\pi}^2 m_\pi} \quad (2.9)$$

resulting in fit parameters $m_{K^*}^2/m_\pi^2$ and $g_{K^*\pi\pi}^2$, both of which are constrained to be non-negative. For the s -wave amplitude we employ a variety of parametrizations. Linear and quadratic parametrizations motivated by analyticity at threshold in E_{cm} and $s = E_{\text{cm}}^2$ (respectively)

$$\begin{aligned} (\tilde{K}_0^{-1})^{\text{LIN}}(E_{\text{cm}}) &= a_{\text{LIN}} + b_{\text{LIN}} E_{\text{cm}}, \\ (\tilde{K}_0^{-1})^{\text{QUAD}}(E_{\text{cm}}) &= a_{\text{QUAD}} + b_{\text{QUAD}} E_{\text{cm}}^2 \end{aligned} \quad (2.10)$$

each have two unconstrained fit parameters. We also include an s -wave parametrization including the first two terms in the effective range expansion

$$(\tilde{K}_0^{-1})^{\text{ERE}}(q_{\text{cm}}) = \frac{-1}{m_\pi a_0} + \frac{m_\pi r_0}{2} \frac{q_{\text{cm}}^2}{m_\pi^2} \quad (2.11)$$

which depends on q_{cm}^2 (rather than E_{cm}) and contains two unconstrained fit parameters $m_\pi a_0$ and $m_\pi r_0$. In addition to these near-threshold parametrizations, we also explore an $\ell = 0$ relativistic Breit-Wigner

$$(\tilde{K}_0^{-1})^{\text{BW}}(E_{\text{cm}}) = \left(\frac{m_{K_0^*}^2}{m_\pi^2} - \frac{E_{\text{cm}}^2}{m_\pi^2} \right) \frac{6\pi m_\pi E_{\text{cm}}}{g_{K_0^*\pi\pi}^2 m_{K_0^*}^2} \quad (2.12)$$

with (non-negative) parameters $m_{K_0^*}^2/m_\pi^2$ and $g_{K_0^*\pi\pi}^2$.

We turn finally to assessment of the systematic error from the truncation to $\ell < 2$. To this end, the determinant condition is simply enlarged to include a d -wave parametrized by the leading-order effective range expansion

$$(\tilde{K}_2^{-1})^{\text{LO}}(E_{\text{cm}}) = -\frac{1}{m_\pi^5 a_2} \quad (2.13)$$

which contains a single unconstrained parameter $m_\pi^5 a_2$. It should be stressed that if $\ell = 2$ partial wave mixing is included, the only irreps which provide one-to-one determinations of the $\ell = 0$ and $\ell = 1$ amplitudes are the $A_{1g}(0)$ and $T_{1u}(0)$, respectively.

3 Results

The formalism discussed in Sec. 2 for determining the finite-volume energies and relating them to the infinite-volume elastic scattering amplitude is applied in this section. Results for the finite-volume energies, B -matrix elements (see Eq. 2.6), and fit parameters for $\tilde{K}_\ell^{-1}(E_{\text{cm}})$ are provided.

3.1 Finite volume energies

Before discussing the results of the ratio fits which are used in the final amplitude analysis, exponential fits to $\hat{C}_n(t)$ are employed to investigate the overlaps of the finite-volume energies onto each of the interpolating operators. While these exponential fits are sometimes less precise and generally suffer from larger excited state contamination compared to ratio fits, they do not require knowledge of suitable nearby non-interacting states and are thereby used to verify ansatze for the ratio fits. To this end, the GEVP eigenvectors from the operator bases listed in Tab. 6 are used to form the overlaps

$$Z_{in}(t) = \left| \frac{\sum_j C_{ij}(t) v_{nj}}{e^{-E_n t/2} \sqrt{\hat{C}_n(t)}} \right|^2 \quad (3.1)$$

where E_n is the energy obtained from single-exponential fits and v_{ni} the i th component of the n th GEVP eigenvector. The $Z_{in}(t)$ (apart from GEVP systematics) plateau to $Z_{in} = |\langle 0 | \hat{O}_i | n \rangle|^2$.

The finite-volume energies from these exponential fits, which are not those used in the final amplitude analysis, are displayed in Fig. 4 together with the overlaps of Eq. 3.1. The overlaps of each interpolating operator onto a single finite-volume eigenstate are typically sharply peaked, indicating that each eigenstate has large overlap onto only one or two interpolating operators. Fig. 4 also demonstrates that the extraction of a few levels above $K\pi\pi$ threshold is possible, however these levels do not have a straight-forward interpretation in terms of infinite-volume scattering amplitudes and are therefore not used in our final analysis.

For the final amplitude analysis, we instead employ the ratio fits. After reconstructing E_{cm} according to Eqs. 2.4 and 2.5, it is used to calculate the B -matrix elements of Eq. 2.6. Depending on the irrep in question, this matrix is either one- or two-dimensional if $\ell \geq 2$ contributions are ignored. The finite-volume energies obtained from the ratio fits and the

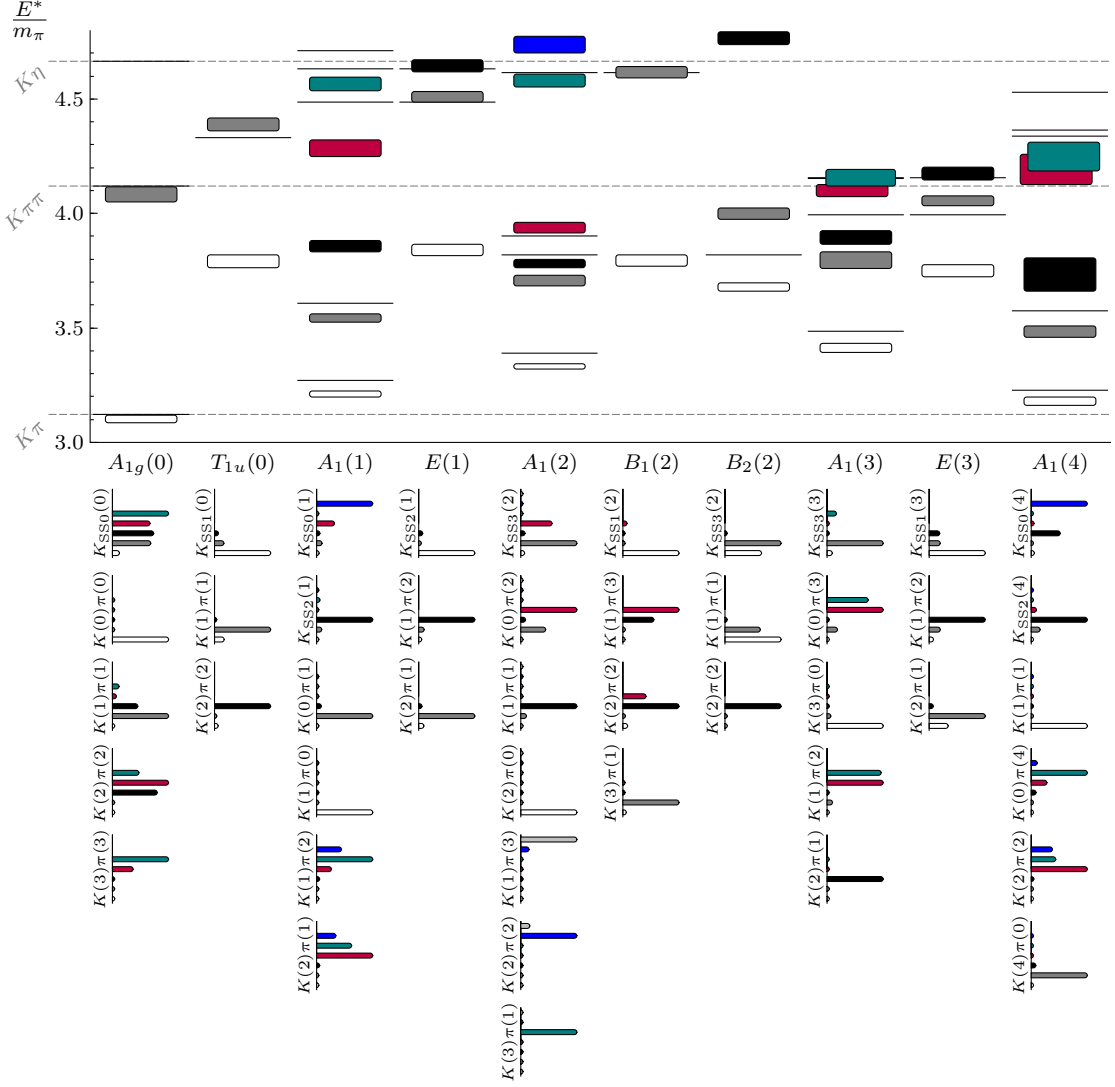


Figure 4: All finite-volume two-hadron energies boosted to the center-of-mass frame determined from single-exponential fits. Each irrep is located in one column, where the energies are shown in the upper panel as boxes with a vertical dimension equal to the statistical error, the non-interacting two-hadron levels as solid horizontal lines, and the relevant thresholds as dashed gray lines. The corresponding columns in the lower panel indicate the overlaps (defined in Eq. 3.1) of each interpolating operator onto the finite-volume Hamiltonian eigenstates. Ratio fits to those levels below $K\pi\pi$ threshold are used in the final analysis.

d^2	Λ	E_{cm}/m_π	\tilde{E}	B_{00}	B_{11}	$\text{Re } B_{01}$	$\text{Im } B_{01}$
0	A_{1g}	3.090(11)	0.9696(23)	3.05(29)	—	—	—
		4.087(23)	1.966(18)	1.48(14)	—	—	—
T_{1u}		3.787(30)	1.666(26)	—	0.094(72)	—	—
1	A_1	3.216(12)	1.0955(46)	1.97(26)	1.28(15)	-1.57(19)	0.0
		3.543(16)	1.4226(81)	0.73(19)	2.07(39)	2.36(25)	0.0
		3.875(23)	1.754(18)	-0.299(53)	-1.438(65)	-0.381(18)	0.0
E		3.848(24)	1.727(20)	—	0.093(52)	—	—
2	A_1	3.346(13)	1.2253(72)	3.4(1.0)	3.6(1.1)	0.0	3.5(1.0)
		3.728(22)	1.607(17)	1.59(41)	0.37(21)	0.0	-1.70(19)
		3.802(18)	1.682(10)	21(29)	4.4(3.9)	0.0	-9(11)
		3.935(23)	1.814(17)	-3.04(82)	-7.4(2.4)	0.0	3.5(1.3)
B_1		3.814(27)	1.694(22)	—	-0.107(40)	—	—
2	B_2	3.676(20)	1.555(12)	—	2.21(28)	—	—
		3.996(21)	1.876(15)	—	-3.56(20)	—	—
3	A_1	3.436(15)	1.315(12)	2.6(1.0)	3.7(1.5)	2.20(86)	2.20(86)
		3.806(37)	1.686(32)	1.06(35)	-0.39(20)	-0.699(13)	-0.699(13)
		3.925(32)	1.805(27)	4.3(2.5)	0.79(48)	-0.66(20)	-0.66(20)
3	E	3.758(41)	1.638(34)	—	1.26(36)	—	—
		4.056(28)	1.936(23)	—	-2.9(3.0)	—	—
4	A_1	3.192(13)	1.0709(52)	2.68(67)	1.24(27)	1.65(42)	0.0
		3.484(19)	1.363(15)	0.67(31)	1.76(54)	-1.84(37)	0.0
		3.721(55)	1.601(53)	-0.77(32)	-1.88(48)	0.99(26)	0.0

Table 4: Finite-volume two-hadron energies in the center-of-mass frame (obtained from ratio fits) together with the corresponding box matrix elements for $\ell < 2$, which are defined in Eq. 2.6. A vanishing matrix element is denoted with a long dash, while some off-diagonal elements are either exactly real or imaginary, with the other component denoted by ‘0.0’. The information included here is used to perform fits using various K -matrix parametrizations.

Fit	<i>s</i> -wave par.	m_{K^*}/m_π	$g_{K^*K\pi}$	$m_\pi a_0$	$\chi^2/\text{d.o.f.}$
(1a,1b)	LIN	3.819(20)	5.54(25)	-0.333(31)	(1.04,-)
2	LIN	3.810(18)	5.30(19)	-0.349(25)	1.49
3	QUAD	3.810(18)	5.31(19)	-0.350(25)	1.47
4	ERE	3.809(17)	5.31(20)	-0.351(24)	1.47
5	BW	3.808(18)	5.33(20)	-0.353(25)	1.42
6	BW	3.810(17)	5.33(20)	-0.354(25)	1.50

Table 5: Results for the $K^*(892)$ resonance parameters and the *s*-wave scattering length $m_\pi a_0$ from all fits to the amplitudes. For each fit, the *p*-wave amplitude is described using the Breit-Wigner of Eq. 2.9. The first row contains results from independent fits to $\ell = 0, 1$ separately, denoted (1a,1b), using only irreps without $\ell = 0, 1$ mixing. This yields a meaningless $\chi^2/\text{d.o.f.}$ for the *s*-wave since there are only two elastic $A_{1g}(0)$ levels. Fit 6 includes *d*-wave contributions as discussed in the text.

$\ell = 0, 1$ *B*-matrix elements are displayed in Tab. 4. This table contains all information (apart from an estimate of covariances, which may be provided on request) required to perform fits to determine $\tilde{K}_\ell(E_{\text{cm}})$.

3.2 *K*-matrix fits

Using the ratio fits and box matrix elements collated in Tab. 4, we turn now to fitting $\tilde{K}_\ell(E_{\text{cm}})$ according to the method outlined in Sec. 2.4. As a basis for comparison, we first employ only irreps in which there is no $\ell = 0, 1$ partial wave mixing and perform independent fits to the *s*- and *p*-waves separately using the Breit-Wigner form of Eq. 2.9 for $\ell = 1$ and the linear form of Eq. 2.10 for $\ell = 0$. These fits are denoted (1a,1b) in Tab. 5. Since there are only two $A_{1g}(0)$ levels in this two-parameter linear *s*-wave fit, the $\chi^2/\text{d.o.f.}$ is meaningless.

Next we consider simultaneous fits to both $\ell = 0, 1$ partial waves. As in fit 1a, the *p*-wave is always described by Eq. 2.9 in these fits, which are also listed in Tab. 5. Fit 2 employs the linear *s*-wave form, fit 3 the quadratic one from Eq. 2.10, fit 4 the NLO effective range expansion of Eq. 2.11 (yielding $m_\pi r_0 = -1.74(31)$), and fit 5 the *s*-wave Breit-Wigner of Eq. 2.12. Fit 6 also employs the *s*-wave Breit-Wigner but enlarges the *K*- and *B*-matrices to include *d*-wave contributions according to Eq. 2.13. Together with the parameters listed in Tab. 5, fit 6 constrains the *d*-wave contribution to be $m_\pi^5 a_2 = -0.0013(68)$.

As is evident from Tab. 5, the $K^*(892)$ resonance parameters are insensitive to the *s*-wave parametrization and the inclusion of *d*-wave contributions. Similarly, if each of the *s*-wave parametrizations are used to interpolate to $K\pi$ threshold and determine the scattering length $m_\pi a_0$, the resulting values also do not vary significantly with different parametrizations or the inclusion of the *d*-wave.

The amplitudes from fit 3 are shown in Fig. 5, together with the Breit-Wigner *s*-wave amplitude from fit 5, illustrating that different parametrizations for the *s*-wave produce a similar energy dependence in the elastic region. In addition to the fits, points from irreps without $\ell = 0, 1$ partial wave mixing are shown and seen to be consistent.

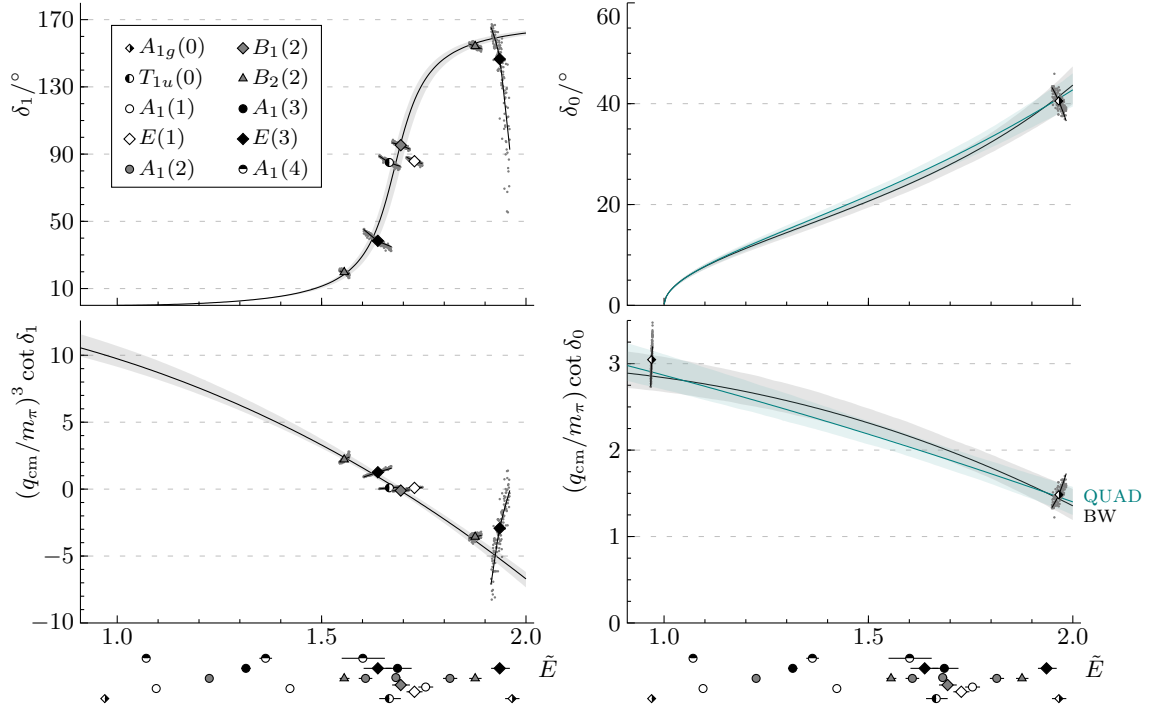


Figure 5: K -matrix fits to the s - and p -wave amplitudes. Together with the fits, which are explained in the text, we show energies (neglecting d -wave contributions) from irreps which do not mix these two partial waves. All energies involved in the fit are indicated below the plots where they are offset vertically for clarity.

We now briefly discuss the s -wave amplitude in the context of the $K_0^*(800)$. Based on the LO effective range expansion, a negative $m_\pi a_0$ suggests a virtual bound state. However, $q_{\text{cm}} \cot \delta_0$ has a significant slope, as is evident in Fig. 5. The NLO effective range parameters of fit 4 are used to construct the ratio $1 - 2r_0/a_0 = -8.9(2.4)$, which must be positive in the presence of a (real or virtual) bound state. A near-threshold bound state is therefore disfavored at the $3 - 4\sigma$ level.

The existence of a resonance pole above threshold on the lower half of the second (unphysical) Riemann sheet requires a careful analytic continuation, and most likely a better energy resolution than we have achieved here. Nonetheless, qualitative information about a possible s -wave pole may be obtained by determining the zeros of $q_{\text{cm}} \cot \delta_0 - iq_{\text{cm}}$. This is easily done using the NLO effective range parametrization of fit 4 and solving the resultant quadratic polynomial, yielding $m_R/m_\pi = 4.66(13) - 0.87(18)i$ which is consistent with the Breit-Wigner mass and width from fit 5, which gives $m_{K_0^*}/m_\pi = 4.59(11)$ and $g_{K_0^* K\pi} = 3.35(17)$. It should be noted that in addition to the $K_0^*(800)$, the s -wave amplitude may also be influenced by the $K_0^*(1430)$ resonance. Overall, without a full analytic continuation we can only infer qualitative information about a possible s -wave resonance pole from the elastic amplitude calculated here.

4 Conclusions

In this work 22 finite-volume $K\pi$ energies calculated from an $N_f = 2 + 1$ lattice QCD simulation are employed to determine the $I = 1/2$, $S = 1$ elastic s - and p -wave $K\pi$ scattering amplitudes. Due to the scattering of non-identical particles, both of these partial waves contribute to finite-volume two-hadron energy shifts in some irreps. We treat this partial wave mixing by fitting both $\ell = 0, 1$ contributions simultaneously, while the $K^*(892)$ resonance parameters and the s -wave scattering length are insensitive to the parametrization chosen for the s -wave and the inclusion of d -wave contributions.

For our values for these quantities we take fit 5 from Tab. 5

$$\frac{m_{K^*}}{m_\pi} = 3.808(18), \quad g_{K^*K\pi} = 5.33(20), \quad m_\pi a_0 = -0.353(25), \quad (4.1)$$

where the errors are statistical only. These values may be compared with existing $K^*(892)$ resonance calculations [38, 52, 71]. Ref. [52] employs a single $N_f = 2$ ensemble with similar (albeit somewhat heavier) pion mass of $m_\pi = 266\text{MeV}$ in a smaller spatial volume with $L = 2\text{fm}$, resulting in four elastic levels from irreps which do not mix with $\ell = 0$. Ref. [71] employs a larger pion mass of $m_\pi = 390\text{MeV}$ and three $N_f = 2 + 1$ ensembles with spatial extents in the range $L = 2 - 3\text{fm}$. At these quark masses the ηK threshold is below $\pi\pi K$, resulting in about 50 two-hadron levels, and a full coupled-channel analysis is performed. Although the $K^*(892)$ is stable but close to threshold at this heavy light quark mass, $q_{\text{cm}}^3 \cot \delta_1$ is nevertheless well described by a Breit-Wigner shape, while analytic continuation of the s -wave amplitude parametrizations suggests a virtual bound state corresponding to the $K_0^*(800)$. Finally, Ref. [38] employs two $N_f = 2$ ensembles with different pion masses ($m_\pi = 150, 160\text{MeV}$) near the physical point and spatial extents $L = 3.5 - 4.6\text{fm}$ in a single amplitude fit. Due to these light quark masses, almost no levels are in the elastic region. A summary of these existing results on $K^*(892)$ resonance parameters is shown in Fig. 6 together with our results. When considering this comparison, one must keep in mind the different scale setting and strange quark mass tuning procedures.

Despite the lack of theoretical control over levels above $K\pi\pi$ threshold, all three of Refs. [38, 52, 71] employ a number of such levels in their amplitude analysis. While one may be tempted to argue that some inelastic levels in Fig. 4 have strong overlap with two hadron interpolators and therefore are well-described by the two-hadron quantization condition of Eq. 2.6, Ref. [78] provides an example (shown there in Fig. 16) where this is not the case. In principle, the formalism developed in Ref. [24] could be adapted to non-identical scalar particles to investigate the magnitude of this systematic error.

For the s -wave amplitude, calculations of $m_\pi a_0$ are considerably more mature than those of the $K^*(892)$ resonance parameters [54, 79–82]. The state-of-the-art for these calculations involves an extrapolation to the continuum and physical quark masses, so comparison with our value is not appropriate. Nonetheless, our value of $m_\pi a_0 = -0.353(25)$ is consistent with expectations from chiral effective theory, shown in Fig. 10 of Ref. [79].

As mentioned above, on this single ensemble we are unable to estimate the magnitude of lattice spacing effects and exponentially suppressed finite-volume corrections to Eq. 2.6, nor are we able to extrapolate the light quark masses to their physical values. This will require a large set of ensembles, such as the CLS ensembles currently employed for an ongoing calculation of the $I = 1$ elastic $\pi\pi$ amplitude which aims to assess these effects [83].

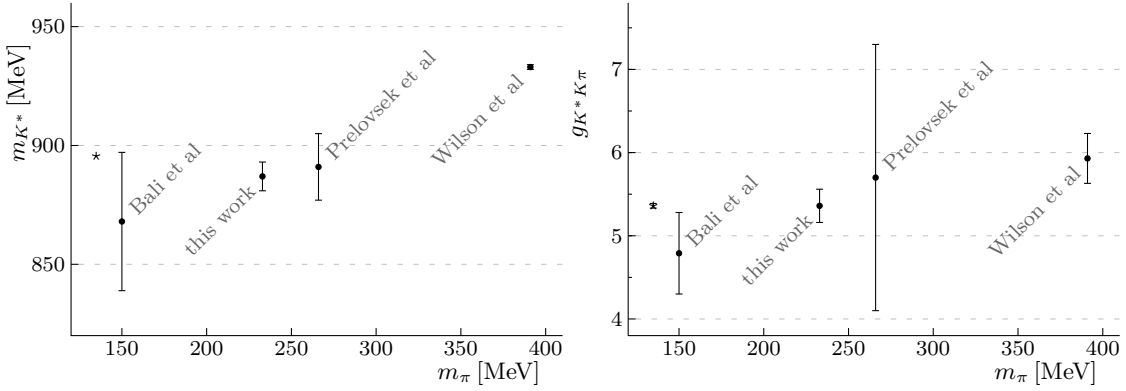


Figure 6: Summary of lattice QCD calculations of $K^*(892)$ resonance parameters, together with phenomenological values (shown as asterisks) from Ref. [6] where the neutral values for the mass and width are taken. This choice gives consistent values to Ref. [38], while hadro-produced $K^*(892)$ parameters result in a coupling which is about 5% larger. The statistical and systematic errors from Ref. [71] are added in quadrature.

Nonetheless, the results reported here are a valuable proof-of-principle and demonstrate the statistical precision which may be attained in such future calculations, although levels near the $K^*(892)$ may exhibit exponential signal-to-noise related degradation in precision as the physical light quark mass is approached. Perhaps a more relevant issue is the decrease of the elastic energy region as the $K\pi\pi$ threshold is lowered to its physical value. To our knowledge, the three-body formalism of Ref. [24] has not yet been applied to numerical lattice data.

Apart from approaching the physical point directly in the lattice simulations, information about physical scattering amplitudes may be inferred from lattice data at heavier quark masses which are however still in the range of applicability of chiral effective theories. This novel interplay between effective field theories and resonant lattice scattering data is currently underway [84–90].

The technology underlying the simultaneous fits performed here to different K -matrix elements is similar to the treatment required for coupled channel problems, on which first calculations have appeared for the $K\pi - K\eta$, $\eta\pi - \bar{K}K$, and $\pi\pi - \eta\eta - \bar{K}K$ systems at a heavier pion mass and smaller physical volume than this work [71]. The methods used here may also be taken over to meson-baryon systems, where the non-zero intrinsic spin provides an additional complication. Nonetheless, first progress on resonant nucleon-pion scattering has been reported recently in Ref. [91].

Acknowledgements: We gratefully acknowledge conversations with D. Mohler and M.F.M. Lutz. This work was supported by the U.S. National Science Foundation under award PHY-1613449. Computing resources were provided by the Extreme Science and Engineering Discovery Environment (XSEDE) under grant number TG-MCA07S017. XSEDE is supported by National Science Foundation grant number ACI-1548562. The USQCD QDP++ library [92] and the Improved BiCGStab solver in Chroma were used in developing the software for early stages of the calculations reported here.

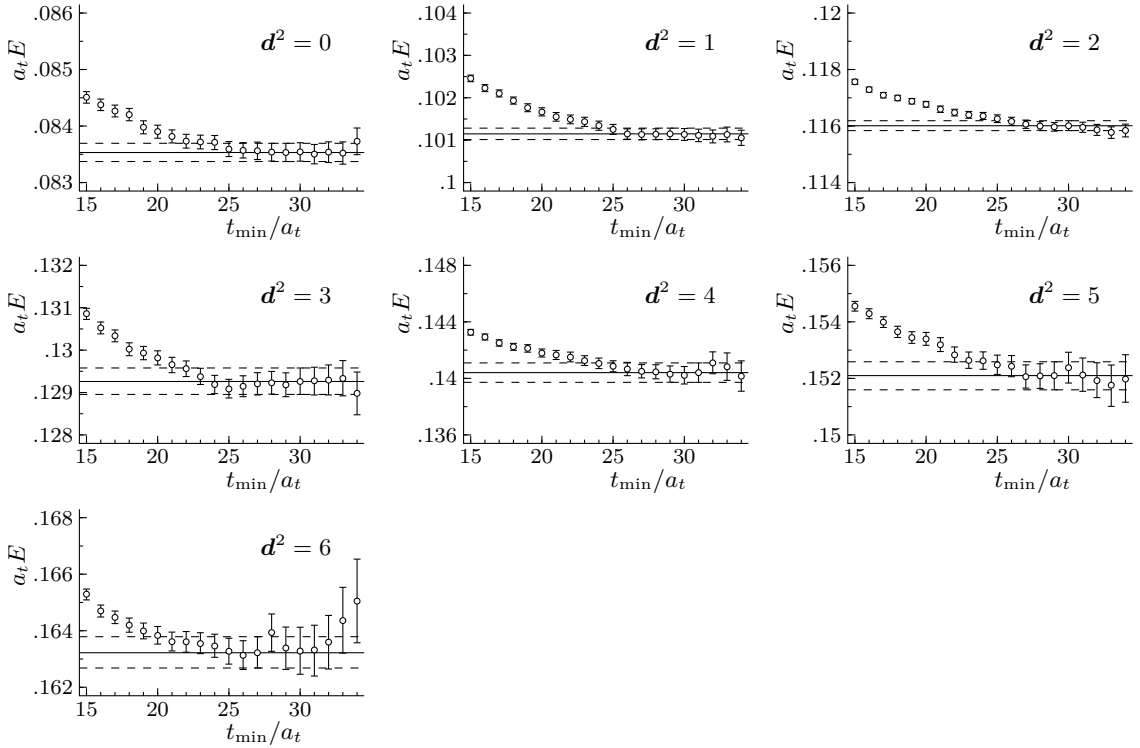


Figure 7: Plots of the t_{\min} dependence of the fitted energies for all moving kaons used to determine ξ_K quoted in Tab. 1 and Fig. 1. For all fits, the maximum time separation is $t_{\max} = 38a_t$.

A t_{\min} -plots for moving kaons

This appendix contains t_{\min} -plots for single exponential fits to each of the moving kaon correlation functions used in determination of the kaon anisotropy ξ_K discussed in Sec. 2.1, which are shown in Fig. 7. As shown in Fig. 1, this determination of ξ_K is consistent with ξ_π determined previously in Ref. [60].

B Operator bases for all irreps

We detail here the basis of interpolating operators used in solving the GEVP of Eq. 2.1 in every irrep. Each operator is constructed to transform irreducibly according to a particular irrep, as detailed in Ref. [77]. While various classes of covariantly displaced operators are considered in Ref. [77], only single-site operators are used here. For each spatial displacement type, a number of linearly independent operators were determined in Ref. [77], each of which is identified by a spatial identification number placed after the spatial displacement type, such as SS0 for the zeroth single-site operator in a particular irrep.

When forming $K\pi$ correlation functions, there is some freedom in choosing the interpolating operators for the constituent pion and kaon. Here we always choose the SS0 operator for all pion and kaon interpolators inside our $K\pi$ operators, except for those with a single unit of momentum where we use the SS1 operators. These compound operators are therefore denoted $K(\mathbf{d}_K^2)\pi(\mathbf{d}_\pi^2)$, where the displacement type and spatial identifica-

d^2	Λ	operators
0	A_{1g}	$K(0)\pi(0), K(1)\pi(1), K(2)\pi(2), K(3)\pi(3), K(0)_{SS0}$
	T_{1u}	$K(0)_{SS1}, K(1)\pi(1), K(2)\pi(2)$
1	A_1	$K(1)\pi(0), K(0)\pi(1), K(1)_{SS2}, K(1)_{SS0}, K(2)\pi(1), K(1)\pi(2)$
	E	$K(1)_{SS2}, K(1)\pi(2), K(2)\pi(1)$
2	A_1	$K(2)\pi(0), K(1)\pi(1), K(2)_{SS3}, K(0)\pi(2), K(3)\pi(1), K(2)\pi(2), K(1)\pi(3)$
	B_1	$K(2)_{SS1}, K(3)\pi(1), K(1)\pi(3), K(2)\pi(2)$
	B_2	$K(2)_{SS3}, K(1)\pi(1), K(2)\pi(2), K(2)_{SS0}$
3	A_1	$K(3)\pi(0), K(3)_{SS3}, K(2)\pi(1), K(0)\pi(3), K(1)\pi(2)$
	E	$K(3)_{SS1}, K(2)\pi(1), K(1)\pi(2)$
4	A_1	$K(1)\pi(1), K(4)\pi(0), K(4)_{SS0}, K(4)_{SS2}, K(0)\pi(4), K(2)\pi(2)$

Table 6: Operator bases included in the GEVP for each two-hadron irrep. Each single-hadron operator is specified by a displacement type and a spatial identification number while the ‘K’ refers only to the flavor structure. The operators used for kaons and pions appearing in two-hadron operators are discussed in the text. The momentum of each operator (in units of $2\pi/L$) squared is shown in parenthesis.

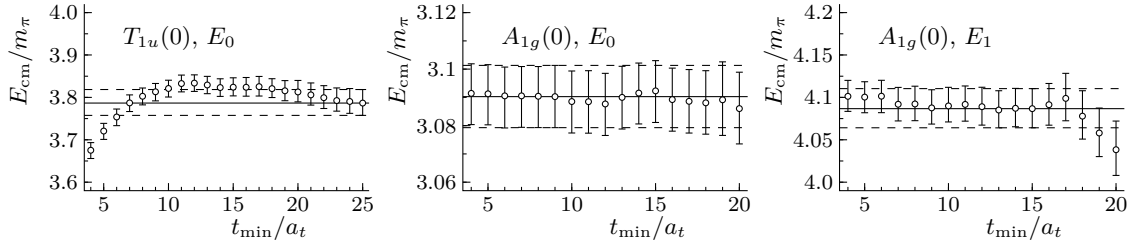


Figure 8: t_{\min} -plots of center-of-mass energy E_{cm} for $d^2 = 0$. The fit value for the chosen t_{\min} is indicated by the error band.

tion number implied and the integers in parenthesis are momenta given in units of $2\pi/L$. Operator identifiers are indicated explicitly for our single-hadron interpolators in Tab. 6.

Coefficient files defining these operators are available upon request, and the list of operators used in each irrep is given in Tab. 6. Each list contains n_{op} operators, while a basis of size $n_{\text{op}} - 1$ is obtained by removing the last operator in the list. These two different bases are used to monitor the stability of the energies, as shown in Fig. 3.

C t_{\min} -plots for all two-hadron levels

Here we show t_{\min} -plots from ratio fits to all two-hadron levels in the amplitude analysis, which employ the GEVP’s specified in App. B. For the $d^2 = 0$ irreps, $t_{\max} = 26a_t$ is employed, while all other fits use $t_{\max} = 35a_t$. Total momentum zero levels are shown in Fig. 8 and those with $d^2 = 1, 2, 3, 4$ in Figs. 9, 10, 11, 12, respectively.

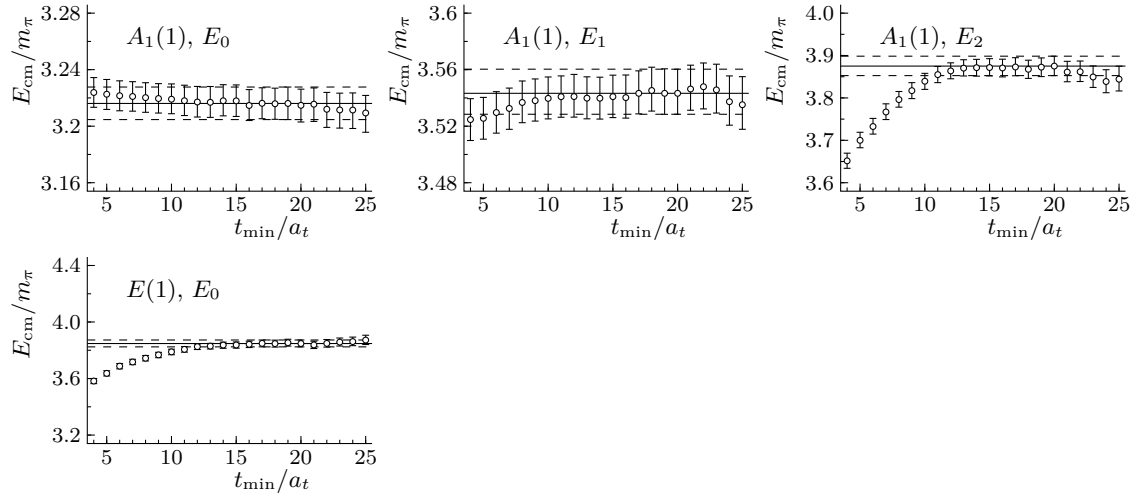


Figure 9: Same as Fig. 8, but for all levels with $d^2 = 1$.

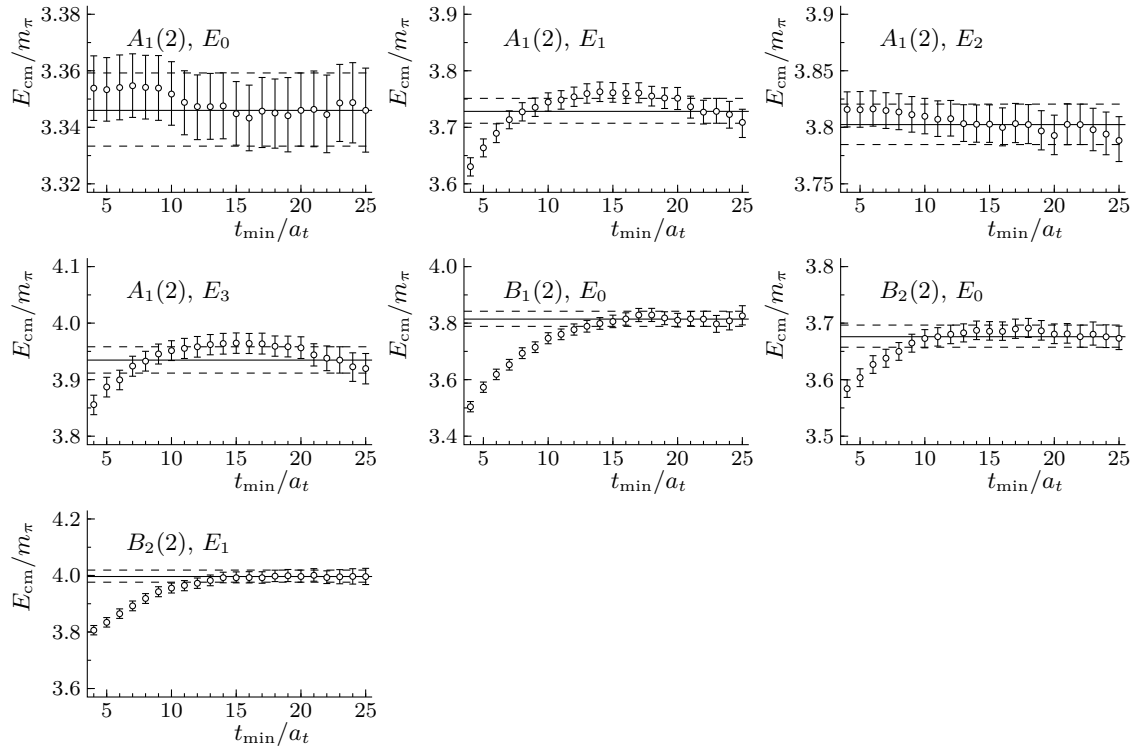


Figure 10: Same as Fig. 8, but for $d^2 = 2$.

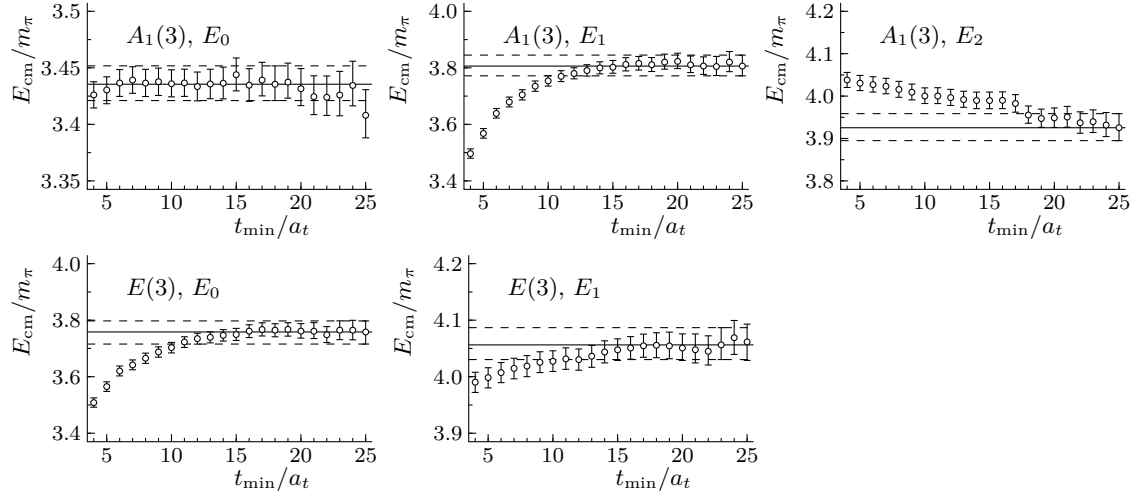


Figure 11: Same as Fig. 8, but for $d^2 = 3$.

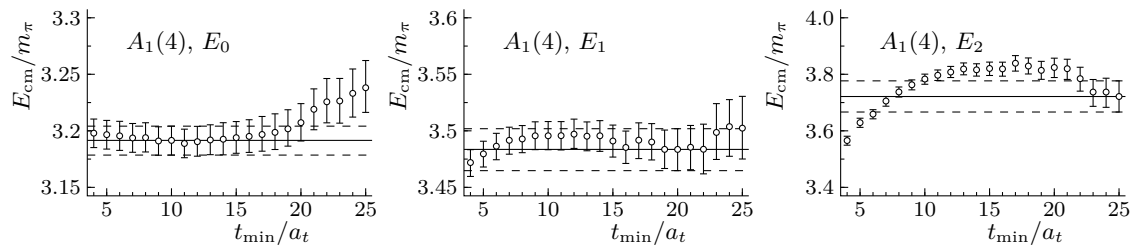


Figure 12: Same as Fig. 8, but for $d^2 = 4$.

References

- [1] **LHCb** Collaboration, R. Aaij et al., *Test of lepton universality with $B^0 \rightarrow K^{*0} \ell^+ \ell^-$ decays*, *JHEP* **08** (2017) 055, [[arXiv:1705.05802](https://arxiv.org/abs/1705.05802)].
- [2] R. R. Horgan, Z. Liu, S. Meinel, and M. Wingate, *Calculation of $B^0 \rightarrow K^{*0} \mu^+ \mu^-$ and $B_s^0 \rightarrow \phi \mu^+ \mu^-$ observables using form factors from lattice QCD*, *Phys. Rev. Lett.* **112** (2014) 212003, [[arXiv:1310.3887](https://arxiv.org/abs/1310.3887)].
- [3] R. R. Horgan, Z. Liu, S. Meinel, and M. Wingate, *Lattice QCD calculation of form factors describing the rare decays $B \rightarrow K^* \ell^+ \ell^-$ and $B_s \rightarrow \phi \ell^+ \ell^-$* , *Phys. Rev.* **D89** (2014), no. 9 094501, [[arXiv:1310.3722](https://arxiv.org/abs/1310.3722)].
- [4] A. Agadjanov, V. Bernard, U.-G. Meißner, and A. Rusetsky, *The $B \rightarrow K^*$ form factors on the lattice*, *Nucl. Phys.* **B910** (2016) 387–409, [[arXiv:1605.03386](https://arxiv.org/abs/1605.03386)].
- [5] L. Lellouch and M. Lüscher, *Weak transition matrix elements from finite volume correlation functions*, *Commun. Math. Phys.* **219** (2001) 31–44, [[hep-lat/0003023](https://arxiv.org/abs/hep-lat/0003023)].
- [6] **Particle Data Group** Collaboration, C. Patrignani et al., *Review of Particle Physics*, *Chin. Phys. C40* (2016), no. 10 100001.
- [7] J. Nebreda and J. R. Pelaez., *Strange and non-strange quark mass dependence of elastic light resonances from $SU(3)$ Unitarized Chiral Perturbation Theory to one loop*, *Phys. Rev.* **D81** (2010) 054035, [[arXiv:1001.5237](https://arxiv.org/abs/1001.5237)].
- [8] I. V. Danilkin, L. I. R. Gil, and M. F. M. Lutz, *Dynamical light vector mesons in low-energy scattering of Goldstone bosons*, *Phys. Lett.* **B703** (2011) 504–509, [[arXiv:1106.2230](https://arxiv.org/abs/1106.2230)].
- [9] **DIRAC** Collaboration, B. Adeva et al., *Observation of $\pi^- K^+$ and $\pi^+ K^-$ atoms*, *Phys. Rev. Lett.* **117** (2016), no. 11 112001, [[arXiv:1605.06103](https://arxiv.org/abs/1605.06103)].
- [10] L. Maiani and M. Testa, *Final state interactions from Euclidean correlation functions*, *Phys. Lett.* **B245** (1990) 585–590.
- [11] M. Lüscher, *Two particle states on a torus and their relation to the scattering matrix*, *Nucl. Phys.* **B354** (1991) 531–578.
- [12] K. Rummukainen and S. A. Gottlieb, *Resonance scattering phase shifts on a nonrest frame lattice*, *Nucl. Phys.* **B450** (1995) 397–436, [[hep-lat/9503028](https://arxiv.org/abs/hep-lat/9503028)].
- [13] M. Göckeler, R. Horsley, M. Lage, U. G. Meißner, P. E. L. Rakow, A. Rusetsky, G. Schierholz, and J. M. Zanotti, *Scattering phases for meson and baryon resonances on general moving-frame lattices*, *Phys. Rev.* **D86** (2012) 094513, [[arXiv:1206.4141](https://arxiv.org/abs/1206.4141)].
- [14] C. Morningstar, J. Bulava, B. Singha, R. Brett, J. Fallica, A. Hanlon, and B. Hörz, *Estimating the two-particle K -matrix for multiple partial waves and decay channels from finite-volume energies*, *Nucl. Phys.* **B924** (2017) 477–507, [[arXiv:1707.05817](https://arxiv.org/abs/1707.05817)].
- [15] R. A. Briceno, Z. Davoudi, and T. C. Luu, *Two-Nucleon Systems in a Finite Volume: (I) Quantization Conditions*, *Phys. Rev.* **D88** (2013), no. 3 034502, [[arXiv:1305.4903](https://arxiv.org/abs/1305.4903)].
- [16] R. A. Briceno, *Two-particle multichannel systems in a finite volume with arbitrary spin*, *Phys. Rev.* **D89** (2014), no. 7 074507, [[arXiv:1401.3312](https://arxiv.org/abs/1401.3312)].
- [17] S. He, X. Feng, and C. Liu, *Two particle states and the S -matrix elements in multi-channel scattering*, *JHEP* **07** (2005) 011, [[hep-lat/0504019](https://arxiv.org/abs/hep-lat/0504019)].
- [18] H. W. Hammer, J. Y. Pang, and A. Rusetsky, *Three particle quantization condition in a finite volume: 2. general formalism and the analysis of data*, [arXiv:1707.02176](https://arxiv.org/abs/1707.02176).

[19] H. W. Hammer, J. Y. Pang, and A. Rusetsky, *Three-particle quantization condition in a finite volume: 1. The role of the three-particle force*, [arXiv:1706.07700](https://arxiv.org/abs/1706.07700).

[20] M. T. Hansen and S. R. Sharpe, *Expressing the three-particle finite-volume spectrum in terms of the three-to-three scattering amplitude*, *Phys. Rev.* **D92** (2015), no. 11 114509, [[arXiv:1504.04248](https://arxiv.org/abs/1504.04248)].

[21] M. T. Hansen and S. R. Sharpe, *Relativistic, model-independent, three-particle quantization condition*, *Phys. Rev.* **D90** (2014), no. 11 116003, [[arXiv:1408.5933](https://arxiv.org/abs/1408.5933)].

[22] M. T. Hansen and S. R. Sharpe, *Applying the relativistic quantization condition to a three-particle bound state in a periodic box*, *Phys. Rev.* **D95** (2017), no. 3 034501, [[arXiv:1609.04317](https://arxiv.org/abs/1609.04317)].

[23] M. T. Hansen and S. R. Sharpe, *Threshold expansion of the three-particle quantization condition*, *Phys. Rev.* **D93** (2016), no. 9 096006, [[arXiv:1602.00324](https://arxiv.org/abs/1602.00324)].

[24] R. A. Briceño, M. T. Hansen, and S. R. Sharpe, *Relating the finite-volume spectrum and the two-and-three-particle S matrix for relativistic systems of identical scalar particles*, *Phys. Rev.* **D95** (2017), no. 7 074510, [[arXiv:1701.07465](https://arxiv.org/abs/1701.07465)].

[25] K. Polejaeva and A. Rusetsky, *Three particles in a finite volume*, *Eur. Phys. J.* **A48** (2012) 67, [[arXiv:1203.1241](https://arxiv.org/abs/1203.1241)].

[26] R. A. Briceno and Z. Davoudi, *Three-particle scattering amplitudes from a finite volume formalism*, *Phys. Rev.* **D87** (2013), no. 9 094507, [[arXiv:1212.3398](https://arxiv.org/abs/1212.3398)].

[27] R. A. Briceño and M. T. Hansen, *Relativistic, model-independent, multichannel $2 \rightarrow 2$ transition amplitudes in a finite volume*, *Phys. Rev.* **D94** (2016), no. 1 013008, [[arXiv:1509.08507](https://arxiv.org/abs/1509.08507)].

[28] R. A. Briceño and M. T. Hansen, *Multichannel $0 \rightarrow 2$ and $1 \rightarrow 2$ transition amplitudes for arbitrary spin particles in a finite volume*, *Phys. Rev.* **D92** (2015), no. 7 074509, [[arXiv:1502.04314](https://arxiv.org/abs/1502.04314)].

[29] R. A. Briceno and Z. Davoudi, *Moving multichannel systems in a finite volume with application to proton-proton fusion*, *Phys. Rev.* **D88** (2013), no. 9 094507, [[arXiv:1204.1110](https://arxiv.org/abs/1204.1110)].

[30] M. T. Hansen and S. R. Sharpe, *Multiple-channel generalization of Lellouch-Luscher formula*, *Phys. Rev.* **D86** (2012) 016007, [[arXiv:1204.0826](https://arxiv.org/abs/1204.0826)].

[31] H. B. Meyer, *Lattice QCD and the Timelike Pion Form Factor*, *Phys. Rev. Lett.* **107** (2011) 072002, [[arXiv:1105.1892](https://arxiv.org/abs/1105.1892)].

[32] M. T. Hansen, H. B. Meyer, and D. Robaina, *From deep inelastic scattering to heavy-flavor semileptonic decays: Total rates into multihadron final states from lattice QCD*, *Phys. Rev.* **D96** (2017), no. 9 094513, [[arXiv:1704.08993](https://arxiv.org/abs/1704.08993)].

[33] S. Hashimoto, *Inclusive semi-leptonic B meson decay structure functions from lattice QCD*, *PTEP* **2017** (2017), no. 5 053B03, [[arXiv:1703.01881](https://arxiv.org/abs/1703.01881)].

[34] **Hadron Spectrum** Collaboration, M. Peardon, J. Bulava, J. Foley, C. Morningstar, J. Dudek, R. G. Edwards, B. Joo, H.-W. Lin, D. G. Richards, and K. J. Juge, *A Novel quark-field creation operator construction for hadronic physics in lattice QCD*, *Phys. Rev.* **D80** (2009) 054506, [[arXiv:0905.2160](https://arxiv.org/abs/0905.2160)].

[35] C. Morningstar, J. Bulava, J. Foley, K. J. Juge, D. Lenkner, M. Peardon, and C. H. Wong, *Improved stochastic estimation of quark propagation with Laplacian Heaviside smearing in lattice QCD*, *Phys. Rev.* **D83** (2011) 114505, [[arXiv:1104.3870](https://arxiv.org/abs/1104.3870)].

[36] R. A. Briceño, J. J. Dudek, and R. D. Young, *Scattering processes and resonances from lattice QCD*, [arXiv:1706.06223](https://arxiv.org/abs/1706.06223).

[37] C. Alexandrou, L. Leskovec, S. Meinel, J. Negele, S. Paul, M. Petschlies, A. Pochinsky, G. Rendon, and S. Syritsyn, *P-wave $\pi\pi$ scattering and the ρ resonance from lattice QCD*, *Phys. Rev.* **D96** (2017), no. 3 034525, [[arXiv:1704.05439](https://arxiv.org/abs/1704.05439)].

[38] **RQCD** Collaboration, G. S. Bali, S. Collins, A. Cox, G. Donald, M. Göckeler, C. B. Lang, and A. Schäfer, *ρ and K^* resonances on the lattice at nearly physical quark masses and $N_f = 2$* , *Phys. Rev.* **D93** (2016), no. 5 054509, [[arXiv:1512.08678](https://arxiv.org/abs/1512.08678)].

[39] Z. Fu and L. Wang, *Studying the ρ resonance parameters with staggered fermions*, *Phys. Rev.* **D94** (2016), no. 3 034505, [[arXiv:1608.07478](https://arxiv.org/abs/1608.07478)].

[40] X. Feng, S. Aoki, S. Hashimoto, and T. Kaneko, *Timelike pion form factor in lattice QCD*, *Phys. Rev.* **D91** (2015), no. 5 054504, [[arXiv:1412.6319](https://arxiv.org/abs/1412.6319)].

[41] X. Feng, K. Jansen, and D. B. Renner, *Resonance Parameters of the ρ -Meson from Lattice QCD*, *Phys. Rev.* **D83** (2011) 094505, [[arXiv:1011.5288](https://arxiv.org/abs/1011.5288)].

[42] K. Orginos, A. Parreno, M. J. Savage, S. R. Beane, E. Chang, and W. Detmold, *Two nucleon systems at $m_\pi \sim 450$ MeV from lattice QCD*, *Phys. Rev.* **D92** (2015), no. 11 114512, [[arXiv:1508.07583](https://arxiv.org/abs/1508.07583)].

[43] **NPLQCD** Collaboration, S. R. Beane, E. Chang, W. Detmold, H. W. Lin, T. C. Luu, K. Orginos, A. Parreno, M. J. Savage, A. Torok, and A. Walker-Loud, *The $I=2$ $\pi\pi$ S-wave Scattering Phase Shift from Lattice QCD*, *Phys. Rev.* **D85** (2012) 034505, [[arXiv:1107.5023](https://arxiv.org/abs/1107.5023)].

[44] C. Pelissier and A. Alexandru, *Resonance parameters of the rho-meson from asymmetrical lattices*, *Phys. Rev.* **D87** (2013), no. 1 014503, [[arXiv:1211.0092](https://arxiv.org/abs/1211.0092)].

[45] **CS** Collaboration, S. Aoki et al., *ρ Meson Decay in 2+1 Flavor Lattice QCD*, *Phys. Rev.* **D84** (2011) 094505, [[arXiv:1106.5365](https://arxiv.org/abs/1106.5365)].

[46] **Hadron Spectrum** Collaboration, J. J. Dudek, R. G. Edwards, and C. E. Thomas, *Energy dependence of the ρ resonance in $\pi\pi$ elastic scattering from lattice QCD*, *Phys. Rev.* **D87** (2013), no. 3 034505, [[arXiv:1212.0830](https://arxiv.org/abs/1212.0830)].

[47] J. J. Dudek, R. G. Edwards, and C. E. Thomas, *S and D-wave phase shifts in isospin-2 $\pi\pi$ scattering from lattice QCD*, *Phys. Rev.* **D86** (2012) 034031, [[arXiv:1203.6041](https://arxiv.org/abs/1203.6041)].

[48] C. B. Lang, D. Mohler, and S. Prelovsek, *$B_s\pi^+$ scattering and search for $X(5568)$ with lattice QCD*, *Phys. Rev.* **D94** (2016) 074509, [[arXiv:1607.03185](https://arxiv.org/abs/1607.03185)].

[49] C. B. Lang, D. Mohler, S. Prelovsek, and R. M. Woloshyn, *Predicting positive parity B_s mesons from lattice QCD*, *Phys. Lett.* **B750** (2015) 17–21, [[arXiv:1501.01646](https://arxiv.org/abs/1501.01646)].

[50] C. B. Lang, L. Leskovec, D. Mohler, S. Prelovsek, and R. M. Woloshyn, *D_s mesons with DK and D^*K scattering near threshold*, *Phys. Rev.* **D90** (2014), no. 3 034510, [[arXiv:1403.8103](https://arxiv.org/abs/1403.8103)].

[51] D. Mohler, C. B. Lang, L. Leskovec, S. Prelovsek, and R. M. Woloshyn, *$D_{s0}^*(2317)$ Meson and D-Meson-Kaon Scattering from Lattice QCD*, *Phys. Rev. Lett.* **111** (2013), no. 22 222001, [[arXiv:1308.3175](https://arxiv.org/abs/1308.3175)].

[52] S. Prelovsek, L. Leskovec, C. Lang, and D. Mohler, *$K\pi$ scattering and the K^* decay width from lattice QCD*, *Phys. Rev.* **D88** (2013), no. 5 054508, [[arXiv:1307.0736](https://arxiv.org/abs/1307.0736)].

[53] D. Mohler, S. Prelovsek, and R. M. Woloshyn, *$D\pi$ scattering and D meson resonances from lattice QCD*, *Phys. Rev.* **D87** (2013), no. 3 034501, [[arXiv:1208.4059](https://arxiv.org/abs/1208.4059)].

[54] C. B. Lang, L. Leskovec, D. Mohler, and S. Prelovsek, *$K\pi$ scattering for isospin 1/2 and 3/2 in lattice QCD*, *Phys. Rev.* **D86** (2012) 054508, [[arXiv:1207.3204](https://arxiv.org/abs/1207.3204)].

[55] C. B. Lang, D. Mohler, S. Prelovsek, and M. Vidmar, *Coupled channel analysis of the ρ meson decay in lattice QCD*, *Phys. Rev.* **D84** (2011), no. 5 054503, [[arXiv:1105.5636](https://arxiv.org/abs/1105.5636)]. [Erratum: *Phys. Rev.* D89,no.5,059903(2014)].

[56] D. Guo, A. Alexandru, R. Molina, and M. Döring, *ρ resonance parameters from lattice QCD*, *Phys. Rev.* **D94** (2016), no. 3 034501, [[arXiv:1605.03993](https://arxiv.org/abs/1605.03993)].

[57] C. Helmes, C. Jost, B. Knippschild, B. Kostrzewa, L. Liu, C. Urbach, and M. Werner, *Hadron-Hadron Interactions from $N_f = 2 + 1 + 1$ lattice QCD: Isospin-1 KK scattering length*, *Phys. Rev.* **D96** (2017), no. 3 034510, [[arXiv:1703.04737](https://arxiv.org/abs/1703.04737)].

[58] L. Liu et al., *Isospin-0 $\pi\pi$ s-wave scattering length from twisted mass lattice QCD*, *Phys. Rev.* **D96** (2017), no. 5 054516, [[arXiv:1612.02061](https://arxiv.org/abs/1612.02061)].

[59] **ETM** Collaboration, C. Helmes, C. Jost, B. Knippschild, C. Liu, J. Liu, L. Liu, C. Urbach, M. Ueding, Z. Wang, and M. Werner, *Hadron-hadron interactions from $N_f = 2 + 1 + 1$ lattice QCD: isospin-2 $\pi\pi$ scattering length*, *JHEP* **09** (2015) 109, [[arXiv:1506.00408](https://arxiv.org/abs/1506.00408)].

[60] J. Bulava, B. Fahy, B. Hörz, K. J. Juge, C. Morningstar, and C. H. Wong, *$I = 1$ and $I = 2$ $\pi - \pi$ scattering phase shifts from $N_f = 2 + 1$ lattice QCD*, *Nucl. Phys.* **B910** (2016) 842–867, [[arXiv:1604.05593](https://arxiv.org/abs/1604.05593)].

[61] M. Fukugita, Y. Kuramashi, M. Okawa, H. Mino, and A. Ukawa, *Hadron scattering lengths in lattice QCD*, *Phys. Rev.* **D52** (1995) 3003–3023, [[hep-lat/9501024](https://arxiv.org/abs/hep-lat/9501024)].

[62] G.-w. Meng, C. Miao, X.-n. Du, and C. Liu, *Lattice study on kaon nucleon scattering length in the $I = 1$ channel*, *Int. J. Mod. Phys.* **A19** (2004) 4401–4412, [[hep-lat/0309048](https://arxiv.org/abs/hep-lat/0309048)].

[63] A. Torok, S. R. Beane, W. Detmold, T. C. Luu, K. Orginos, A. Parreno, M. J. Savage, and A. Walker-Loud, *Meson-Baryon Scattering Lengths from Mixed-Action Lattice QCD*, *Phys. Rev.* **D81** (2010) 074506, [[arXiv:0907.1913](https://arxiv.org/abs/0907.1913)].

[64] W. Detmold and A. Nicholson, *Low energy scattering phase shifts for meson-baryon systems*, *Phys. Rev.* **D93** (2016), no. 11 114511, [[arXiv:1511.02275](https://arxiv.org/abs/1511.02275)].

[65] C. Lang and V. Verduci, *Scattering in the πN negative parity channel in lattice QCD*, *Phys. Rev.* **D87** (2013), no. 5 054502, [[arXiv:1212.5055](https://arxiv.org/abs/1212.5055)].

[66] C. B. Lang, L. Leskovec, M. Padmanath, and S. Prelovsek, *Pion-nucleon scattering in the Roper channel from lattice QCD*, *Phys. Rev.* **D95** (2017), no. 1 014510, [[arXiv:1610.01422](https://arxiv.org/abs/1610.01422)].

[67] G. Moir, M. Peardon, S. M. Ryan, C. E. Thomas, and D. J. Wilson, *Coupled-Channel $D\pi$, $D\eta$ and $D_s\bar{K}$ Scattering from Lattice QCD*, *JHEP* **10** (2016) 011, [[arXiv:1607.07093](https://arxiv.org/abs/1607.07093)].

[68] R. A. Briceno, J. J. Dudek, R. G. Edwards, and D. J. Wilson, *Isoscalar $\pi\pi$ scattering and the σ meson resonance from QCD*, *Phys. Rev. Lett.* **118** (2017), no. 2 022002, [[arXiv:1607.05900](https://arxiv.org/abs/1607.05900)].

[69] R. A. Briceño, J. J. Dudek, R. G. Edwards, C. J. Shultz, C. E. Thomas, and D. J. Wilson, *The $\pi\pi \rightarrow \pi\gamma^*$ amplitude and the resonant $\rho \rightarrow \pi\gamma^*$ transition from lattice QCD*, *Phys. Rev.* **D93** (2016), no. 11 114508, [[arXiv:1604.03530](https://arxiv.org/abs/1604.03530)].

[70] **Hadron Spectrum** Collaboration, J. J. Dudek, R. G. Edwards, and D. J. Wilson, *An a_0 resonance in strongly coupled $\pi\eta$, $K\bar{K}$ scattering from lattice QCD*, *Phys. Rev.* **D93** (2016), no. 9 094506, [[arXiv:1602.05122](https://arxiv.org/abs/1602.05122)].

[71] D. J. Wilson, R. A. Briceno, J. J. Dudek, R. G. Edwards, and C. E. Thomas, *Coupled $\pi\pi$, $K\bar{K}$ scattering in P-wave and the ρ resonance from lattice QCD*, *Phys. Rev.* **D92** (2015), no. 9 094502, [[arXiv:1507.02599](https://arxiv.org/abs/1507.02599)].

[72] D. J. Wilson, J. J. Dudek, R. G. Edwards, and C. E. Thomas, *Resonances in coupled $\pi K, \eta K$ scattering from lattice QCD*, *Phys. Rev.* **D91** (2015), no. 5 054008, [[arXiv:1411.2004](https://arxiv.org/abs/1411.2004)].

[73] **Hadron Spectrum** Collaboration, H.-W. Lin et al., *First results from 2+1 dynamical quark flavors on an anisotropic lattice: Light-hadron spectroscopy and setting the strange-quark mass*, *Phys. Rev.* **D79** (2009) 034502, [[arXiv:0810.3588](https://arxiv.org/abs/0810.3588)].

[74] R. G. Edwards, B. Joo, and H.-W. Lin, *Tuning for Three-flavors of Anisotropic Clover Fermions with Stout-link Smearing*, *Phys. Rev.* **D78** (2008) 054501, [[arXiv:0803.3960](https://arxiv.org/abs/0803.3960)].

[75] C. Michael and I. Teasdale, *Extracting Glueball Masses From Lattice QCD*, *Nucl. Phys.* **B215** (1983) 433.

[76] J. Foley, K. Jimmy Juge, A. O'Cais, M. Peardon, S. M. Ryan, and J.-I. Skullerud, *Practical all-to-all propagators for lattice QCD*, *Comput. Phys. Commun.* **172** (2005) 145–162, [[hep-lat/0505023](https://arxiv.org/abs/hep-lat/0505023)].

[77] C. Morningstar, J. Bulava, B. Fahy, J. Foley, Y. Jhang, et al., *Extended hadron and two-hadron operators of definite momentum for spectrum calculations in lattice QCD*, *Phys. Rev.* **D88** (2013), no. 1 014511, [[arXiv:1303.6816](https://arxiv.org/abs/1303.6816)].

[78] P. Giudice, D. McManus, and M. Peardon, *A comparison of analysis techniques for extracting resonance parameters from lattice Monte Carlo data*, *Phys. Rev.* **D86** (2012) 074516, [[arXiv:1204.2745](https://arxiv.org/abs/1204.2745)].

[79] Z. Fu, *Lattice study on πK scattering with moving wall source*, *Phys. Rev.* **D85** (2012) 074501, [[arXiv:1110.1422](https://arxiv.org/abs/1110.1422)].

[80] T. Janowski, P. A. Boyle, A. Jüttner, and C. Sachrajda, *$K - \pi$ scattering lengths at physical kinematics*, *PoS LATTICE2014* (2014) 080.

[81] S. R. Beane, P. F. Bedaque, T. C. Luu, K. Orginos, E. Pallante, A. Parreno, and M. J. Savage, *πK scattering in full QCD with domain-wall valence quarks*, *Phys. Rev.* **D74** (2006) 114503, [[hep-lat/0607036](https://arxiv.org/abs/hep-lat/0607036)].

[82] **PACS-CS** Collaboration, K. Sasaki, N. Ishizuka, M. Oka, and T. Yamazaki, *Scattering lengths for two pseudoscalar meson systems*, *Phys. Rev.* **D89** (2014), no. 5 054502, [[arXiv:1311.7226](https://arxiv.org/abs/1311.7226)].

[83] J. Bulava, B. Hörz, and C. Morningstar, *Multi-hadron spectroscopy in a large physical volume*, in *35th International Symposium on Lattice Field Theory (Lattice 2017) Granada, Spain, June 18-24, 2017*. [arXiv:1710.04545](https://arxiv.org/abs/1710.04545).

[84] B. Hu, R. Molina, M. Döring, M. Mai, and A. Alexandru, *Chiral extrapolations of the $\rho(770)$ meson in $N_f = 2 + 1$ lattice QCD simulations*, *Phys. Rev.* **D96** (2017), no. 3 034520, [[arXiv:1704.06248](https://arxiv.org/abs/1704.06248)].

[85] D. R. Bolton, R. A. Brécn, and D. J. Wilson, *Connecting physical resonant amplitudes and lattice QCD*, *Phys. Lett.* **B757** (2016) 50–56, [[arXiv:1507.07928](https://arxiv.org/abs/1507.07928)].

[86] Z.-W. Liu, J. M. M. Hall, D. B. Leinweber, A. W. Thomas, and J.-J. Wu, *Structure of the $\Lambda(1405)$ from Hamiltonian effective field theory*, *Phys. Rev.* **D95** (2017), no. 1 014506, [[arXiv:1607.05856](https://arxiv.org/abs/1607.05856)].

[87] Z.-W. Liu, W. Kamleh, D. B. Leinweber, F. M. Stokes, A. W. Thomas, and J.-J. Wu, *Hamiltonian effective field theory study of the $N^*(1440)$ resonance in lattice QCD*, *Phys. Rev.* **D95** (2017), no. 3 034034, [[arXiv:1607.04536](https://arxiv.org/abs/1607.04536)].

[88] A. Martinez Torres, E. Oset, S. Prelovsek, and A. Ramos, *An analysis of the Lattice QCD spectra for $D_{s0}^*(2317)$ and $D_{s1}^*(2460)$* , in *17th International Conference on Hadron Spectroscopy and Structure (Hadron 2017) Salamanca, Spain, September 25-29, 2017*, 2017. [arXiv:1712.09468](https://arxiv.org/abs/1712.09468).

- [89] Z.-H. Guo, L. Liu, U.-G. Meißner, J. A. Oller, and A. Rusetsky, *Chiral study of the $a_0(980)$ resonance and $\pi\eta$ scattering phase shifts in light of a recent lattice simulation*, *Phys. Rev. D* **95** (2017), no. 5 054004, [[arXiv:1609.08096](https://arxiv.org/abs/1609.08096)].
- [90] X.-Y. Guo, Y. Heo, and M. F. M. Lutz, *On the chiral extrapolation of charmed meson masses*, [arXiv:1801.10122](https://arxiv.org/abs/1801.10122).
- [91] C. W. Andersen, J. Bulava, B. Hörz, and C. Morningstar, *Elastic $I = 3/2$, p -wave nucleon-pion scattering amplitude and the $\Delta(1232)$ resonance from $N_f=2+1$ lattice QCD*, *Phys. Rev. D* **97** (2018), no. 1 014506, [[arXiv:1710.01557](https://arxiv.org/abs/1710.01557)].
- [92] **SciDAC** Collaboration, R. G. Edwards and B. Joo, *The Chroma software system for lattice QCD*, *Nucl. Phys. Proc. Suppl.* **140** (2005) 832.